Zeolite Crystallization

DOI: 10.1002/anie.201107725

Tailoring Silicalite-1 Crystal Morphology with Molecular Modifiers**

*Alexandra I. Lupulescu and Jeffrey D. Rimer**

The shape-selectivity of zeolites can be exploited for commercial applications in catalysis, ion-exchange, and separations by the judicious selection of crystal structures with nanopore geometries commensurate with sorbate molecules.[1] Zeolites tend to form anisotropic crystals with pore openings presented on low surface area faces and channels oriented axially along the longest crystal dimensions, which limit molecule access to pores on exterior crystal surfaces and increase the internal path length for molecular diffusion. These factors impose severe mass transport limitations that reduce molecular flux and decrease the yield, selectivity, and/or lifetime of zeolite catalysts, which poses a pervasive challenge to optimize zeolite crystal morphology. As such, a strategic aim is to design more effective, facile, and inexpensive synthetic pathways to selectively tailor crystal habit with precise and predictive control.

There are several approaches that can be used to modify zeolite morphology. Adjustments to synthesis conditions, such as molar composition, solvent, pH, and temperature, have marginal effects on the kinetics and thermodynamics of crystal growth.[2] Templates, such as surfactants, gels, and porous solids can be used to synthesize crystals with a morphology that mimics spatial features of the template.[3] A third approach is the design of structure-directing agents (SDAs) capable of tuning crystal size and oriented growth.[4] Studies of novel SDAs have elegantly demonstrated the impact of crystal engineering on zeolite performance (i.e. structure–function relationships)[4a,5] and the synthesis of new frameworks;[6] however, high costs associated with multistep SDA synthesis and the inability to recycle SDAs due to their thermal decomposition during zeolite post-treatment limits the commercial viability of this technique.

Here we report a novel, bio-inspired method of tailoring zeolite morphology by using zeolite growth modifiers (ZGMs), which are molecules with a specificity for binding to select crystal faces and altering the anisotropic rates of surface step growth.[7] This method is a new approach in zeolite shape engineering, whereby a priori knowledge of ZGM molecular recognition can be used to achieve unparalleled control of zeolite morphology. This rational approach, which is unique to zeolite synthesis, is ubiquitous in biological systems where modifiers (e.g. proteins) mediate the rate of crystal nucleation and growth. Such interactions are responsible for the mechanism by which cold weather species prevent ice formation using antifreeze proteins, which bind to ice crystals through epitaxial H-bonding and entropic hydrophobic interactions.[8] Additional examples of modifier–crystal interactions include the formation of mollusk shells (calcite), human bone (hydroxyapatite), and pathological diseases such as kidney stones and atherosclerosis.[9] Modifiers are used in the oil and gas industry to inhibit the crystallization of minerals (e.g. $BaSO_4$).[10] Biomimetic modifiers have been used to direct the assembly of oxides (TiO_2, amorphous silica, etc.)[11] with a range of shapes and sizes. Moreover, Rimer et al. applied this concept to design synthetic modifiers as viable drug targets for cystinuria (a genetic kidney stone disease caused by L-cystine crystallization).[12]

The mechanism of growth inhibition is illustrated in Figure 1 A. Modifiers adsorbed on crystal surfaces block the attachment of growth units, thereby reducing the rate of growth normal to the surface. A challenge of this design approach is identifying modifiers with molecular recognition for specific crystal faces. To this end, our choice to select ZGMs was derived from the functional moieties of silica proteins, termed silicateins or silaffins, which mediate the assembly of silica exoskeletons in unicellular sponges and diatoms, respectively (Figure 1 B).[13] These hierarchical architectures assemble at ambient conditions through interactions between a silica interface and proteins rich in amine (primary to tertiary), phosphate, and hydroxyamino acid groups.

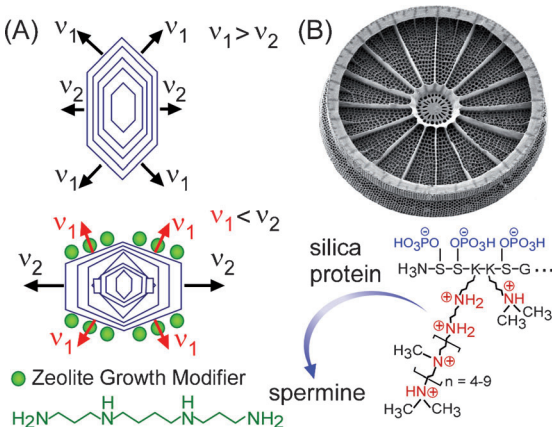

Figure 1. A) Native crystal habit (top) can be modified (bottom) by using molecules that bind to specific surfaces and alter anisotropic growth. B) The amorphous silica exoskeletons of diatoms are formed through interactions with amine-rich proteins, which we mimic in silicalite-1 synthesis by using synthetic ZGM analogues.[14]

[*] A. I. Lupulescu, Prof. J. D. Rimer
Department of Chemical and Biomolecular Engineering, University of Houston, 4800 Calhoun Rd., Houston, TX 77204-4004 (USA)
E-mail: jrimer@central.uh.edu
Homepage: http://www.chee.uh.edu/faculty/rimer/main

[**] We are grateful to the National Science Foundation (CBET-1032621) for funding. We would like to thank N. Thai, M. Diosomito, and M. Oleksiak for help with data collection.

Supporting information for this article is available on the WWW under http://dx.doi.org/10.1002/anie.201107725.

Modifiers generally possess two moieties:[15] a "binder" that interacts with crystal surface sites and a "perturber" that sterically hinders the attachment of growth units. Effective modifiers closely mimic crystal surface features and orient in solute vacancies by hydrogen-bond, van der Waals, or electrostatic interactions. Zeolite growth near equilibrium is described by a layer-by-layer model,[16] in which hillocks nucleate with well-defined steps that advance across the surface by the addition of growth units to step sites (Figure 2).

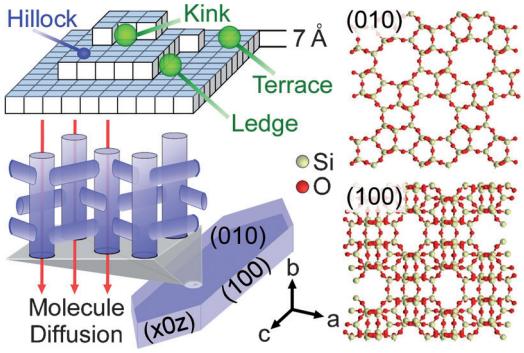

Figure 2. Silicalite-1 (MFI structure) has straight and sinusoidal channels oriented in the *b* [010] and *a* [100] directions, respectively. The rates of hillock nucleation and step advancement are influenced by ZGM binding to terrace, ledge, or kink sites on crystal surfaces.

Modifiers that bind to kink sites are the most potent inhibitors of step advancement (i.e. exhibit high efficacy at low concentrations). Modifiers that bind to ledge sites also reduce the rate of step growth, while those adsorbed on terrace sites inhibit hillock nucleation. In synthesis conditions that promote surface roughening, such as high supersaturation,[17] studies of biominerals have shown that macromolecule modifiers (e.g. polymers) are more effective growth inhibitors than smaller molecules (e.g. monomers) due to their proximal binding groups that block layer nucleation and reduce step propagation through step pinning mechanisms.[18]

For this study we selected the zeolite silicalite-1, the siliceous analogue of ZSM-5, which has a MFI framework structure consisting of intersecting straight and sinusoidal channels (Figure 2). Silicalite-1 crystals exhibit hexagonal platelet morphologies with two distinct surfaces, the (010) and (100) faces, and a third surface, (*x*0*z*), with variable Miller index. Straight channels oriented along the [010] direction present the least tortuous path for sorbate diffusion. As such, a desired outcome of MFI shape-engineering is the design of thin platelets with reduced length along [010] pores to increase the diffusional flux of sorbate molecules. Indeed, Tsapatsis et al. showed that *b*-oriented silicalite-1 films markedly enhanced the flux and selectivity of *p*-/*o*-xylene separations.[4a] Likewise, Ryoo et al. showed that ultrathin ZSM-5 platelets with a ca. 2 nm [010] diffusion path length noticeably improved catalytic performance.[5a]

Here we used atomic force microscopy (AFM) to examine the interaction of ZGM functional groups with silicalite-1 crystals (Figure 3). AFM has proven useful for probing ligand–receptor interactions[19] in biological systems through

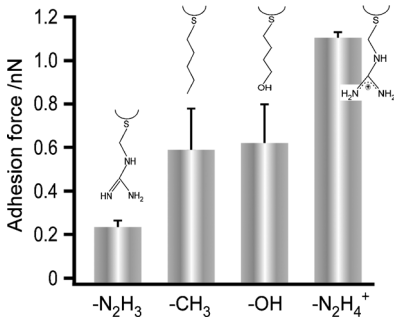

Figure 3. AFM adhesion force between Au-coated AFM tips modified with a layer of organothiols and the silicalite-1 (010) surface. The thiol terminal groups mimic ZGM moieties. A pH 12 solution was used for $-$OH and $-CH_3$ tips, and pH 11 ($-N_2H_4^+$) and pH 13 ($-N_2H_3$) were used for amidinium tips. Each force is an average from 8000 pull-off curves on multiple crystals (error bars equal one standard deviation).

the measurement of the unbinding force (or adhesion force, F_A) of tips modified with proteins or peptides. AFM force spectroscopy measures changes in the deflection, Δz, of a cantilever with an appropriately modified tip as it is retracted from a contacting surface, thereby producing a pull-off curve with $F_A \alpha \Delta z$. This technique was used to identify strong modifier binding moieties to help guide the design of ZGMs. Notably, we tested modified AFM tips that mimic silaffin functional groups, such as cationic amines, hydroxy groups, and hydrophobic residues. Measurements were performed in alkaline solution to examine the adhesion force between negatively charged (010) surfaces (i.e. SiOH $pK_a < 11$)[20] and functionalized AFM tips (see Supporting Information for details). A trend of increasing F_A was observed for different tip functional groups: amidinium (neutral charge) < methyl ≈ alcohol < amidinium (positive charge). Alcohol groups can form H-bonds with surface silanols, while methyl groups can bury into vacancies on the crystal surface to remove entropically unfavorable solvent layers. AFM tips modified with amidinium groups ($pK_a \approx 12.1$) exhibit neutral or positive charge depending on the pH. Tips with positively charged amidinium groups exhibit a 6-fold increase in F_A relative to neutral tips. To our knowledge, this is the first AFM force spectroscopy study of zeolite surfaces.

The influence of ZGMs on silicalite-1 growth was assessed by bulk crystallization studies. Additives were introduced to synthesis solutions prior to hydrothermal treatment using tetraethylorthosilicate (TEOS) as the silica source and tetrapropylammonium (TPA^+) as the SDA. The first modifier selected for these studies was spermine ($C_{10}H_{26}N_4$), which is an exact mimic of an amine segment of long-chain polyamines found in diatom cells (Figure 1 B and Supporting Information, Figure S10). Figure 4 compares SEM images of silicalite-1 crystals synthesized in the presence of modifiers. We observed that spermine reduces the thickness of MFI platelets by a factor of 4 (Figure 4 A), consistent with a preferential binding of spermine to basal (010) faces, which reduces the rate of growth along the *b*-axis. The second modifier tested was triethylenetetramine (TETA, $C_6H_{18}N_4$), which has a structure that is similar to spermine, but with fewer carbonyl groups. Interestingly, TETA proved to be much less effective

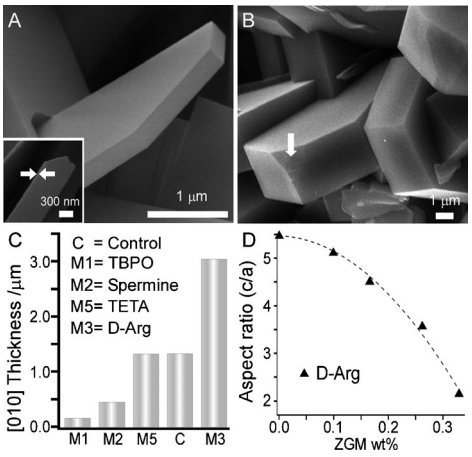

Figure 4. Effect of modifiers on silicalite-1 crystal morphology. SEM images reveal crystals synthesized with <0.5 wt% spermine (A) and D-Arg (B) have decreased and increased thickness, respectively. C) ZGMs selectively tailor the thickness of silicalite-1 platelets along the *b*-axis (i.e. diffusion length in less tortuous [010] channels). D) D-Arg preferentially binds to (302) faces, causing a monotonic reduction in the *c*/*a* (length/width) aspect ratio of basal (010) faces with increasing D-Arg wt%.

at inhibiting silicalite-1 [010] growth (Figure 4C), which emphasizes how subtle changes in molecular structure impact ZGM efficacy.

We used dynamic light scattering (DLS) to measure temporal changes in the hydrodynamic diameter of silicalite-1 crystals in the presence of spermine (Figure 5). DLS studies reveal that the rate of crystal growth decreases linearly with spermine concentration (Figure S4). Moreover, spermine produced a narrower particle size distribution and fewer surface defects (crystal twinning) compared to the control (Figure S11). Over 30 additional commercial molecules were tested in silicalite-1 growth studies to assess their efficacy and specificity (Table S4). These molecules were selected with functional groups similar to silica proteins. The silicalite-1 platelet length, *c*-axis, and width, *a*-axis, were measured by optical microscopy. Analyses revealed that modifiers preferentially bind to the (100) and ($x0z$) surfaces to increase or

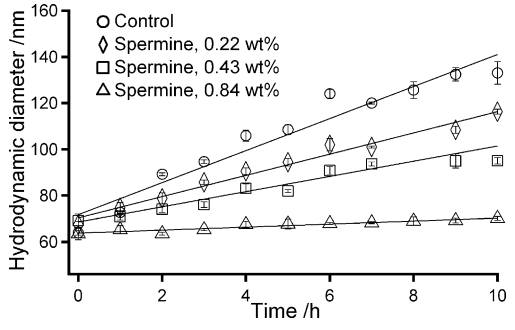

Figure 5. DLS seeded growth experiments measuring the temporal change in the hydrodynamic diameter of silicalite-1 seeds suspended in a silica growth solution at 85 °C. The growth rate (slope) decreases linearly with increasing spermine concentration. Experimental data (symbols) are an average of four measurements and error bars equal two standard deviations. Lines are linear regression.

decrease the *c*/*a* aspect ratio, respectively (Figure S12). A systematic study of the dihedral angles in scanning electron micrographs reveals that the ($x0z$) index varies with synthesis conditions (Table S6). The ($x0z$) surface is often mislabeled in the literature as the (101) face, which is true for select cases, but is more commonly the (201) or (503) surface. ZGMs direct the formation of new facets, including the (302) face and a non-indexed face (Figure 4B, arrow) that is unique to syntheses with the amino acid D-arginine (D-Arg). The latter is a potent inhibitor of the [302] growth rate, as evidenced by the monotonic decrease in *c*/*a* aspect ratio with increasing D-Arg concentration (Figure 4D), wherein a 2.5-fold reduction in aspect ratio is achieved with less than 0.3 wt% D-Arg. We also observed nonspecific ZGM-crystal interactions, which yielded a constant *c*/*a* aspect ratio with *a*- and *c*-dimensions that are either smaller or larger than the control. This suggests ZGMs influence crystal number density (i.e. nucleation), which we are currently investigating.

We screened the library of molecules in Table S4 for the most efficient modifiers of silicalite-1 [010] thickness. The ZGM with the highest efficacy was tributylphosphine oxide (TBPO), which produced μm-sized platelets in the *ac*-plane with a thickness less than 150 nm in the *b*-axis; however, TBPO phase separates in aqueous solution at appreciable concentrations (>0.3 wt%). As mentioned, spermine is an efficient modifier and yielded slightly thicker platelets than TBPO. D-Arg had an opposite effect, leading to a marked increase in platelet thickness (Figure 4C) and reduction in platelet length (*c*-axis). Collectively, bulk crystallization studies reveal that modifier(s) with molecular recognition for specific crystal surfaces can tune anisotropic growth rates to achieve 3-dimensional control of silicalite-1 crystal shape.

A systematic analysis of silicalite-1 crystals by AFM provides microscopic validation of the phenomena observed in the bulk crystallization studies. AFM images of silicalite-1 (010) surfaces reveal hillocks with a 0.7 nm step height, which corresponds to the dimension of a pentasil chain (a structural subunit of MFI). Images of silicalite-1 control surfaces reveal triangular hillocks with a step density $\rho = 30\ \mu m^{-2}$ (Figure 6A). Modifiers that preferentially bind to (010) surfaces block the attachment of growth units, thus reducing the rate of hillock nucleation and decreasing ρ. Indeed, we observe two- and four-fold reductions in step density on silicalite-1 crystals grown in the presence of spermine and TBPO, respectively. This is consistent with bulk crystallization studies that reveal TBPO is the more potent inhibitor of growth along the [010] direction.

Modifiers that preferentially bind to (010)∩(100) or (010)∩($x0z$) ledge sites on the basal surface inhibit step advancement across the (010) plane. Since ZGM adsorption at step sites does not affect hillock nucleation on terraces, a reduction in step velocity leads to higher ρ. This phenomenon was observed with several modifiers, including tris(hydroxymethyl)aminomethane (THAM, $C_4H_{11}NO_3$), which produced a large step density ($\rho \approx 80\ \mu m^{-2}$). THAM binding to silicalite-1 ledge sites also altered the hillock morphology from the characteristic triangular shape of control crystals (Figure 6A) to more rounded, elliptical-shaped islands (Figure 6C).

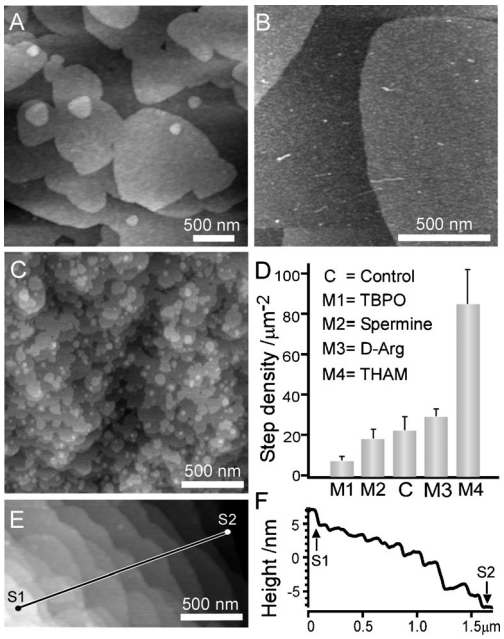

Figure 6. AFM height images of silicalite-1 (010) surfaces for the A) control (no additive) and those synthesized with B) TBPO, C) THAM, and E) D-Arg modifiers. D) Comparison of the (010) step density for different ZGMs (error bars = 1 standard deviation). F) Height cross-section of image (E) (line) reveals step bunches (single step = 0.7 nm).

Stoyanov and Michailov[21] derived the relationship $\rho \alpha N^{-1/2}$ for multinuclear layer-by-layer growth where N is the number of nuclei (i.e. layers on a crystal surface). Syntheses with D-Arg produced silicalite-1 crystals with a small fraction of single steps and a larger population of step bunches (Figure 6F) with average step heights of 1.7 nm (i.e. two pentasil layers). Differences in step height for D-Arg ($N = 2$) and THAM ($N = 1$) account for the expected factor of four difference in ρ. Classical theories of crystal growth also predict an inverse relationship $v \alpha h^{-1}$ between the step height, h, and the velocity of step advancement, v. This is consistent with the observed increase in [010] growth due to the preferential binding of D-Arg to (302) surfaces, which produces step bunches that advance across the (010) surface with reduced velocity, $v_{[302]}$.

A comparison of D-Arg and THAM modifiers reveals that their effect on ρ is determined not only by ZGM specificity, but also its binding strength to silicalite-1 surfaces. The effect of THAM on silicalite-1 growth is much less pronounced than D-Arg, which can be attributed to weaker THAM-crystal binding as well as the competitive adsorption between modifier and TPA^+ on silicalite-1 surfaces. Growth solutions with 0.2 wt% ZGM contain ca. 15 moles of TPA^+ for every one mole of ZGM. If the strength of ZGM binding to silicalite-1 surfaces is weaker or comparable to that of TPA^+, the latter will have a higher surface coverage. As the free concentration of TPA^+ in solution decreases with synthesis time (due to SDA occlusion in MFI pores), ZGM coverage on silicalite-1 surfaces will increase. Likewise, silica supersaturation decreases with synthesis time. Collectively, both effects reduce the rate of step advancement; and if step growth is slow relative to nucleation, fewer step bunches and higher ρ are observed (Figure 6C). The lack of step bunching is consistent with classical models of crystal growth, which invoke the power-law dependence $R \alpha \sigma^n$ for the rate of step growth, R, and the solute (silica) supersaturation, σ. As the silicalite-1 synthesis approaches equilibrium ($\sigma \approx 1$), hillocks on (010) terraces do not grow fast enough to generate step bunches. To test this hypothesis, we increased the concentration of THAM in silicalite-1 syntheses to 3.7 wt% (2 TPA^+:1 THAM) and observed an appreciable increase in platelet thickness (Figure S15) and step bunching (i.e. reduced ρ). This suggests THAM has a higher coverage on silicalite-1 surfaces at earlier times in the synthesis (when $\sigma \gg 1$), which is qualitatively consistent with theory and the trends observed in Figure S15C.

In summary, we have shown that commercially available zeolite growth modifiers can be used to selectively control the anisotropic growth rates of silicalite-1 crystallization. Through the judicious selection of ZGMs with molecular recognition for specific crystal faces, this method offers versatility in using a single modifier or mixture of modifiers (acting cooperatively) to realize unparalleled 3-dimensional control of crystal morphology. ZGMs offer a straightforward and effective method to tailor the kinetics of crystallization wherein molecules can be designed with steric bulk to prevent their occlusion in zeolite pores, which permits recycling. Indeed, elemental analysis of silicalite-1 with 4.7 wt% TBPO (Table S6) reveals the amount of modifier in extracted solid crystals is negligible. In addition, preliminary studies of other framework structures, such as mordenite, reveal that crystal morphology can be altered in the presence of ZGMs (Figure S16). A critical challenge remains in identifying fundamental aspects of ZGM-crystal molecular recognition. To this end, we are exploring the design of new modifiers and are using molecular modeling to understand their binding modes on different crystal surfaces to develop heuristic guidelines for rational zeolite design. Collectively, these studies suggest a generalized utility of ZGMs for tailoring nanoporous materials with optimal crystal morphologies for a wide range of applications through a sophisticated yet facile, cost-effective technique.

Experimental Section

Silicalite-1 was prepared from a clear solution of molar composition 40 TEOS:40 TPAOH:9420 H_2O:160 EtOH where growth modifiers were added to solutions prior to heating (160 °C for 65 h). DLS measurements were performed by using seeded growth solutions of molar composition 8 TEOS:7 TPAOH:9500 H_2O:32 EtOH. AFM studies were performed on an Asylum Research SA-MFP-3D. Adhesion force measurements employed AFM tips (Olympus, Au-coated) functionalized with organothiols. A detailed description of the experimental methods is provided in the Supporting Information.

Received: November 2, 2011
Published online: January 17, 2012

Keywords: adhesion force · crystal engineering · growth modifiers · molecular recognition · zeolites

[1] C. Martínez, A. Corma, *Coord. Chem. Rev.* **2011**, *255*, 1558 – 1580.

[2] T. O. Drews, M. Tsapatsis, *Curr. Opin. Colloid Interface Sci.* **2005**, *10*, 233 – 238.

[3] a) S. J. Lee, D. F. Shantz, *Chem. Mater.* **2005**, *17*, 409 – 417; b) W. C. Yoo, S. Kumar, R. L. Penn, M. Tsapatsis, A. Stein, *J. Am. Chem. Soc.* **2009**, *131*, 12377 – 12383; c) R. R. Mukti, H. Hirahara, A. Sugawara, A. Shimojima, T. Okubo, *Langmuir* **2010**, *26*, 2731 – 2735.

[4] a) Z. Lai, G. Bonilla, I. Diaz, J. G. Nery, K. Sujaoti, M. A. Amat, E. Kokkoli, O. Terasaki, R. W. Thompson, M. Tsapatsis, D. G. Vlachos, *Science* **2003**, *300*, 456 – 460; b) G. Bonilla, I. Diaz, M. Tsapatsis, H. K. Jeong, Y. Lee, D. G. Vlachos, *Chem. Mater.* **2004**, *16*, 5697 – 5705; c) J. Kecht, S. Mintova, T. Bein, *Chem. Mater.* **2007**, *19*, 1203 – 1205; d) J. Kecht, S. Mintova, T. Bein, *Langmuir* **2008**, *24*, 4310 – 4315.

[5] a) M. Choi, K. Na, J. Kim, Y. Sakamoto, O. Terasaki, R. Ryoo, *Nature* **2009**, *461*, 246 – U120; b) K. Varoon, X. Y. Zhang, B. Elyassi, D. D. Brewer, M. Gettel, S. Kumar, J. A. Lee, S. Maheshwari, A. Mittal, C. Y. Sung, M. Cococcioni, L. F. Francis, A. V. McCormick, K. A. Mkhoyan, M. Tsapatsis, *Science* **2011**, *334*, 72 – 75.

[6] R. Simancas, D. Dari, N. Velamazan, M. T. Navarro, A. Cantin, J. L. Jorda, G. Sastre, A. Corma, F. Rey, *Science* **2010**, *330*, 1219 – 1222.

[7] a) L. Addadi, Z. Berkovitchyellin, I. Weissbuch, J. Vanmil, L. J. W. Shimon, M. Lahav, L. Leiserowitz, *Angew. Chem.* **1985**, *97*, 476 – 496; *Angew. Chem. Int. Ed. Engl.* **1985**, *24*, 466 – 485; b) I. Weissbuch, L. Addadi, M. Lahav, L. Leiserowitz, *Science* **1991**, *253*, 637 – 645.

[8] a) A. C. Doxey, M. W. Yaish, M. Griffith, B. J. McConkey, *Nat. Biotechnol.* **2006**, *24*, 852 – 855; b) S. P. Graether, M. J. Kuiper, S. M. Gagne, V. K. Walker, Z. C. Jia, B. D. Sykes, P. L. Davies, *Nature* **2000**, *406*, 325 – 328.

[9] a) J. S. Evans, *Chem. Rev.* **2008**, *108*, 4455 – 4462; b) F. C. Meldrum, H. Colfen, *Chem. Rev.* **2008**, *108*, 4332 – 4432; c) R. C. Johnson, J. A. Leopold, J. Loscalzo, *Circ. Res.* **2006**, *99*, 1044 – 1059; d) P. Fratzl, R. Weinkamer, *Prog. Mater. Sci.* **2007**, *52*, 1263 – 1334.

[10] E. Mavredaki, A. Neville, K. S. Sorbie, *Cryst. Growth Des.* **2011**, *11*, 4751 – 4758.

[11] a) M. B. Dickerson, K. H. Sandhage, R. R. Naik, *Chem. Rev.* **2008**, *108*, 4935 – 4978; b) J. N. Cha, G. D. Stucky, D. E. Morse, T. J. Deming, *Nature* **2000**, *403*, 289 – 292; c) F. Rodríguez, D. D. Glawe, R. R. Naik, K. P. Hallinan, M. O. Stone, *Biomacromolecules* **2004**, *5*, 261 – 265; d) J. S. Jan, D. F. Shantz, *Adv. Mater.* **2007**, *19*, 2951 – 2956.

[12] J. D. Rimer, Z. An, Z. Zhu, M. H. Lee, J. A. Wesson, D. S. Goldfarb, M. D. Ward, *Science* **2010**, *330*, 337 – 341.

[13] a) J. Aizenberg, J. C. Weaver, M. S. Thanawala, V. C. Sundar, D. E. Morse, P. Fratzl, *Science* **2005**, *309*, 275 – 278; b) N. Kroger, S. Lorenz, E. Brunner, M. Sumper, *Science* **2002**, *298*, 584 – 586; c) Y. Zhou, K. Shimizu, J. N. Cha, G. D. Stucky, D. E. Morse, *Angew. Chem.* **1999**, *111*, 825 – 828; *Angew. Chem. Int. Ed.* **1999**, *38*, 779 – 782.

[14] Scanning electron micrographs of the silica diatom (Figure 1 B) and sponge (table of content) were provided by Photo Researchers Inc.

[15] J. P. Sizemore, M. F. Doherty, *Cryst. Growth Des.* **2009**, *9*, 2637 – 2645.

[16] W. A. Tiller, *The Science of Crystallization*: *Microscopic Phenomena and Defect Generation*, Cambridge University Press, Ithaca, **1991**.

[17] M. W. Anderson, T. Ohsuna, Y. Sakamoto, Z. Liu, A. Carlsson, O. Terasaki, *Chem. Commun.* **2004**, 907 – 916.

[18] T. Jung, X. X. Sheng, C. K. Choi, W. S. Kim, J. A. Wesson, M. D. Ward, *Langmuir* **2004**, *20*, 8587 – 8596.

[19] a) D. J. Müller, M. Krieg, D. Alsteens, Y. F. Dufrene, *Curr. Opin. Biotechnol.* **2009**, *20*, 4 – 13; b) X. X. Sheng, T. S. Jung, J. A. Wesson, M. D. Ward, *Proc. Natl. Acad. Sci. USA* **2005**, *102*, 267 – 272.

[20] J. D. Rimer, R. F. Lobo, D. G. Vlachos, *Langmuir* **2005**, *21*, 8960 – 8971.

[21] S. Stoyanov, M. Michailov, *Surf. Sci.* **1988**, *202*, 109 – 124.

